A self-enhanced chemiexcited PDT system for targeted and efficient treatment of deeply seated tumors

Xuwen Da,[a] Yunli Xu,[a,b] Lei Wang,[c] Xiulian Liu,[a,b] Yatong Peng,[a,b] Yao Wu,[a,b] Wanpeng Zhou,[a,b] Wentao Wang,[*c] Xuesong, Wang,[*a,b] Qianxiong Zhou[*a]

[a]Key Laboratory of Photochemical Conversion and Optoelectronic Materials, Technical Institute of Physics and Chemistry, Chinese Academy of Sciences, Beijing 100190, China

[b]University of Chinese Academy of Sciences, Beijing 100049, China

[c]Wenzhou Institute, University of Chinese Academy of Sciences, Wenzhou 325000, China

*__Corresponding e-mail address__: wangwentao@ucas.ac.cn, xswang@mail.ipc.ac.cn, zhouqianxiong@mail.ipc.ac.cn

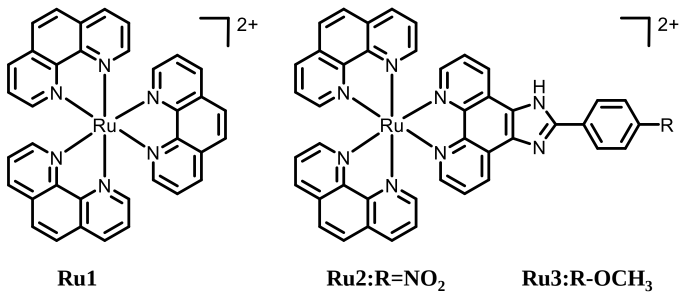

Scheme S1. Chemical structures of Ru1-Ru3.

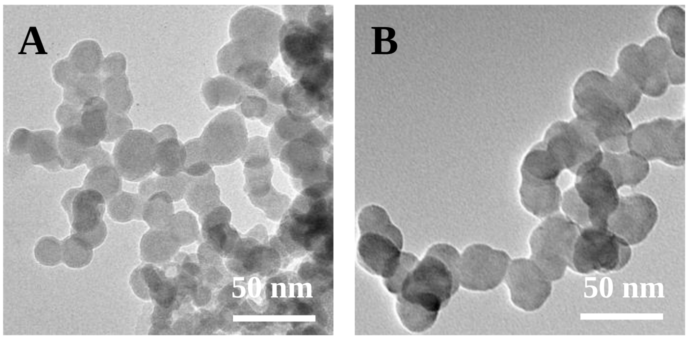

Fig.S1. TEM images of NP1 (A) and NP2 (B).

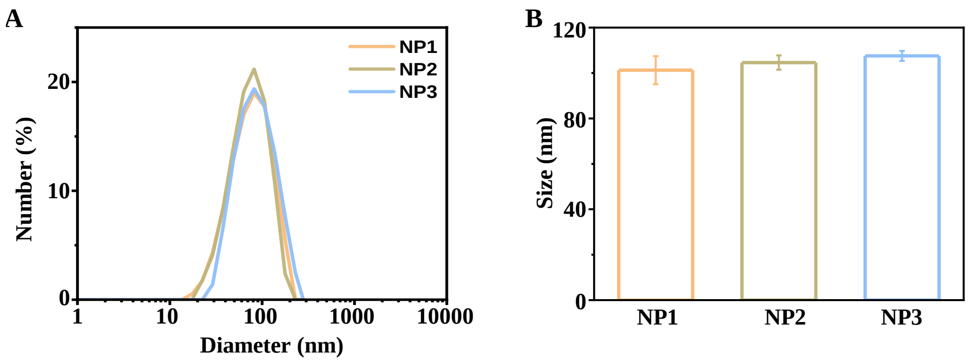

Fig.S2. DLS results of NP1, NP2 and NP3.

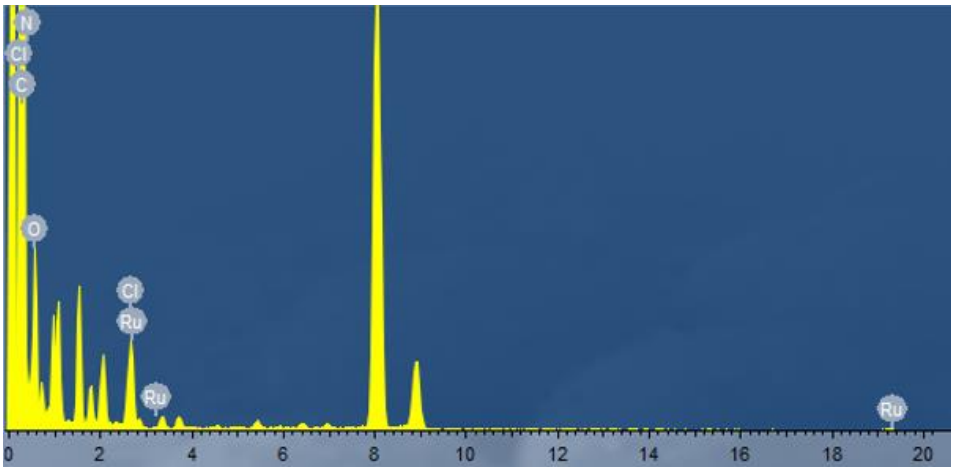

Fig.S3. An EDS spectrum of NP3.

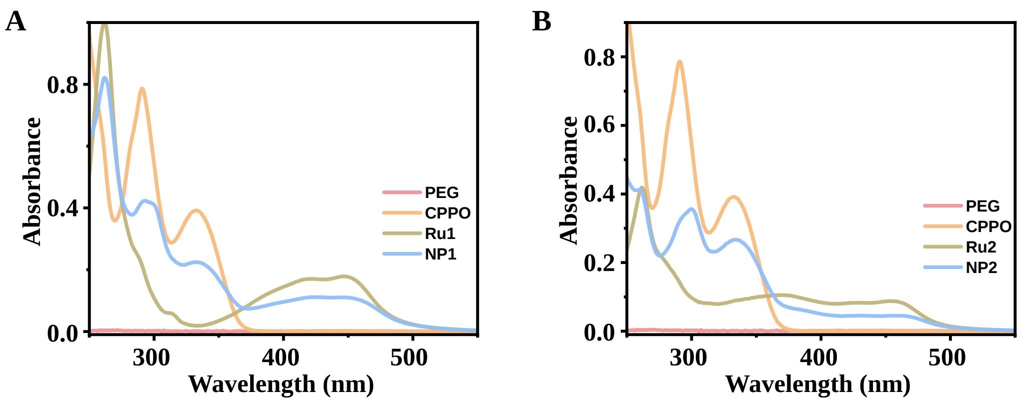

Fig.S4. Absorption spectra of NP1, Ru1, CPPO and PEG (A), and NP2, Ru2, CPPO and PEG (B) in H_2O.

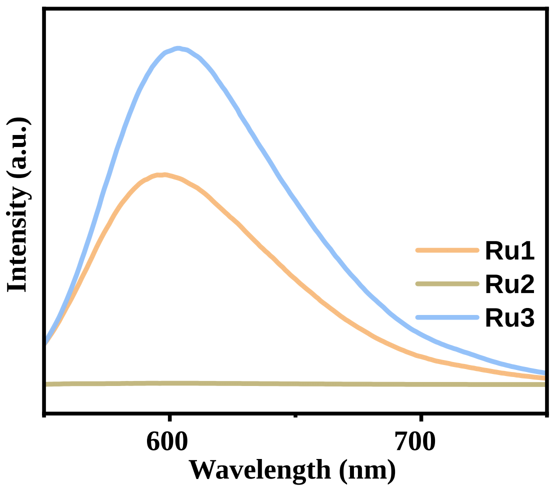

Fig.S5. Emission spectra of Ru1, Ru2 and Ru3 in H_2O.

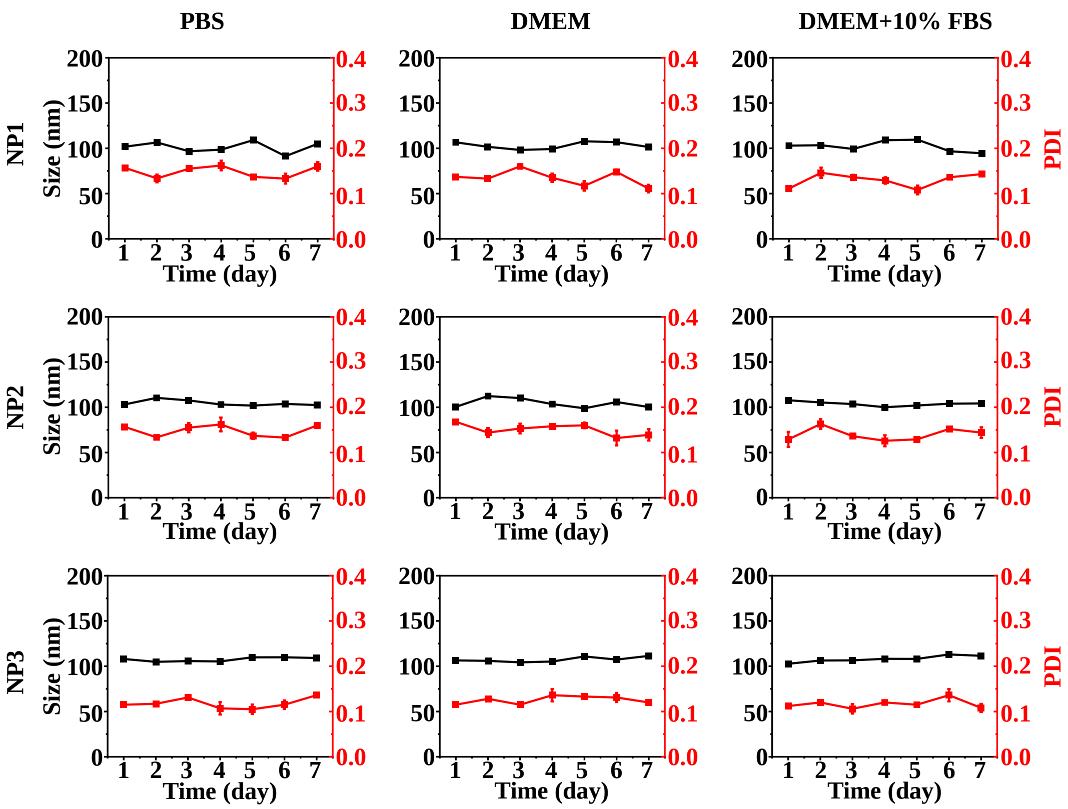

Fig.S6. The DLS results of NP1, NP2 and NP3 in PBS, DMEM and DMEM + 10% FBS for 7 days.

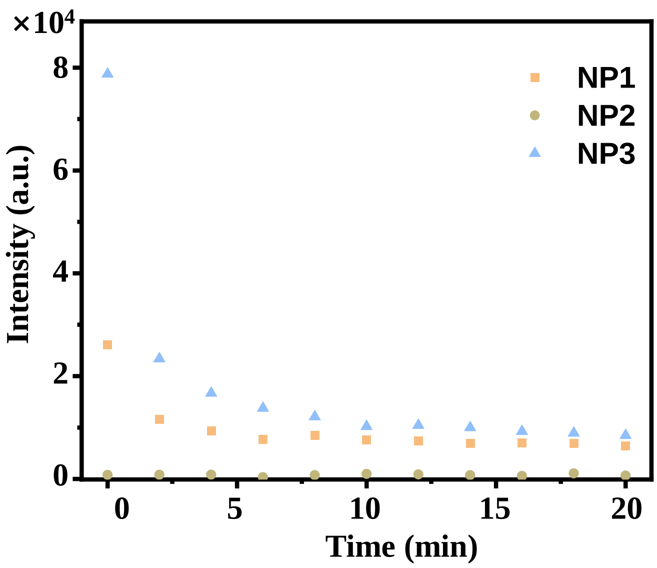

Fig.S7. Chemiluminescence intensity of NP1-NP3 (10 μM based on Ru1-Ru3) in the presence of H_2O_2 (1 mM) at different time.

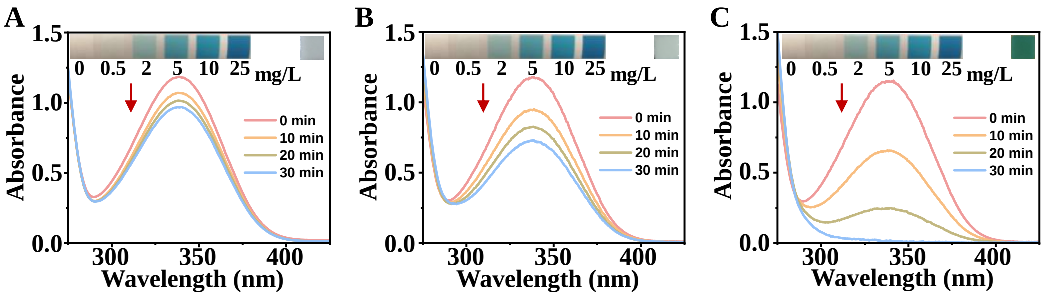

Fig.S8. Absorption spectral changes of NADH (200 μM) in the presence of Ru1 (A), Ru2 (B) and Ru3 (0.5 μM) under light irradiation (470 nm, 22.5 mW cm^{-2}) in H_2O. Inset was the color development of H_2O_2 test paper after irradiation.

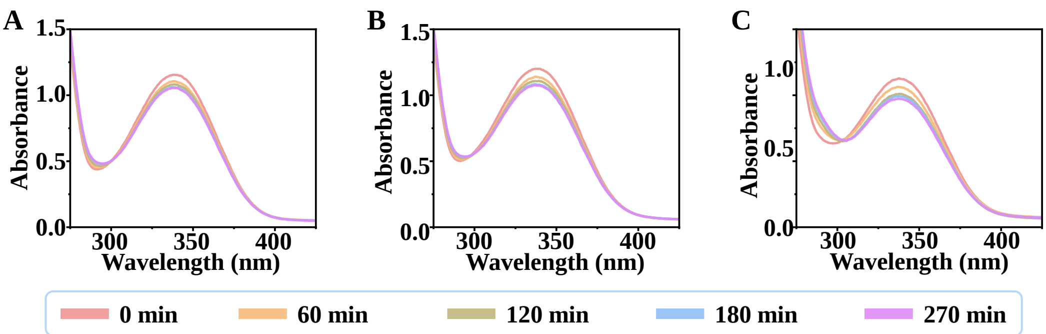

Fig.S9. Absorption spectral changes of NADH (200 μM) treated with NP1 (A), NP2 (B) and NP3 (C) (2 μM based on Ru1-Ru3) in H_2O without H_2O_2.

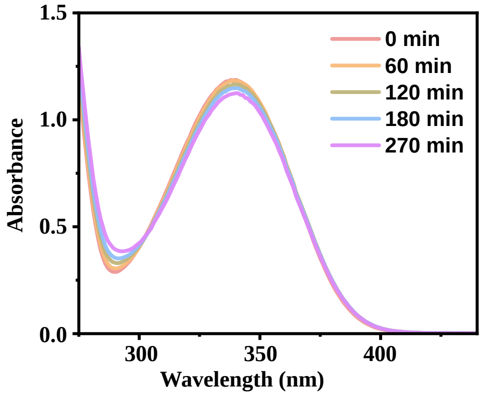

Fig.S10. Absorption spectral changes of NADH (200 μM) treated with only H_2O_2 (200 μM) in H_2O.

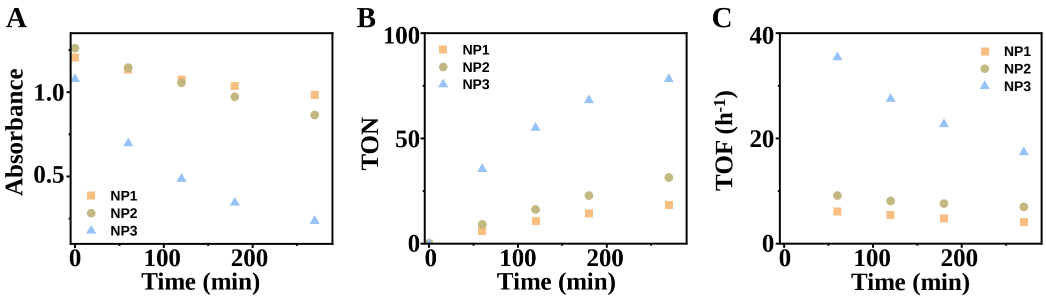

Fig.S11. (A) Absorption intensity changes of NADH (200 μM) at 336 nm in the presence of NP1-NP3 (2 μM based on Ru1-Ru3) and 200 μM H_2O_2 in water; (B) Turnover number (TON) values of NP1-NP3 (based on the concentration of Ru1-Ru3) for NADH oxidation at different times; (C) Turnover frequency (TOF) values of NP1-NP3 (based on the concentration of Ru1-Ru3) for NADH oxidation at different times.

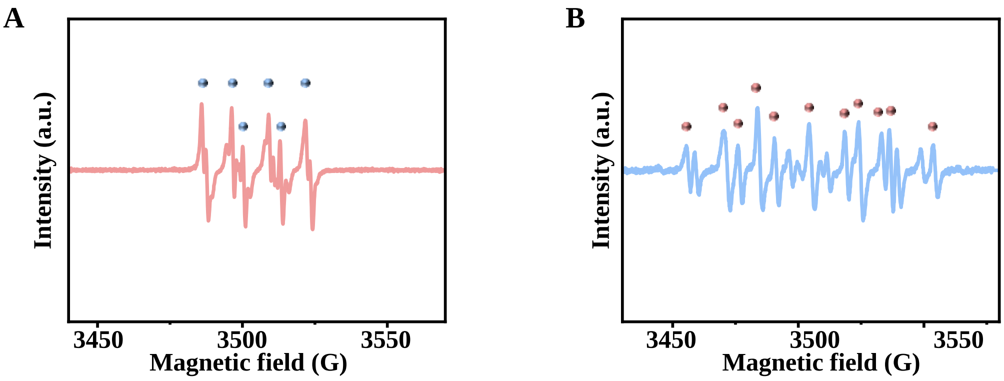

Fig.S12. (A) An EPR spectrum of the mixture of NP3 (4 μM based on Ru3), NADH (200 μM) and H_2O_2 (200 μM) in H_2O using DMPO (20 mM) as the $O_2^{\cdot -}$ trapping agent; (B) An EPR spectrum of $NAD^{\bullet}$ radical in the presence of NP3 (50 μM based on Ru3), H_2O_2 (2.5 mM), NADH (2.5 mM) using CYPMPO (2 mM) as the trapping agent in a methanol/PBS (1:1) solution.

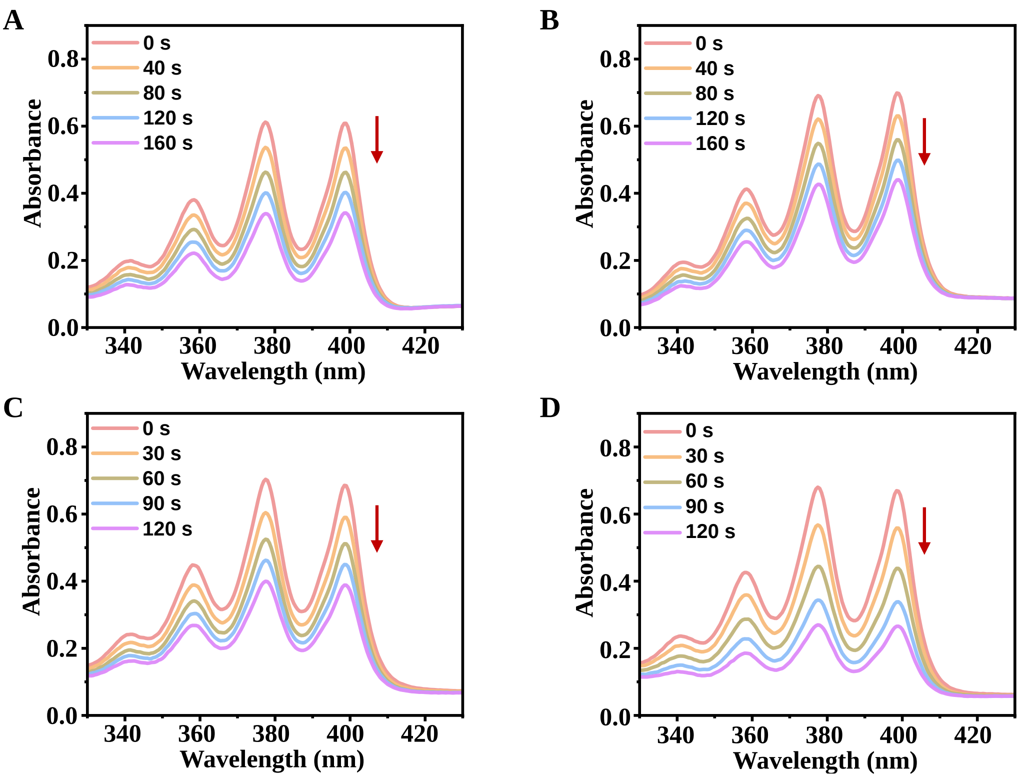

Fig.S13. $^1O_2$ generation of $Ru(bpy)_3^{2+}$ (A), Ru1 (B), Ru2 (C), and Ru3 (D) in water upon 470 nm light irradiation (22.5 mW/cm^2), using 9,10-ABDA (50 μM) as a chemical trap.

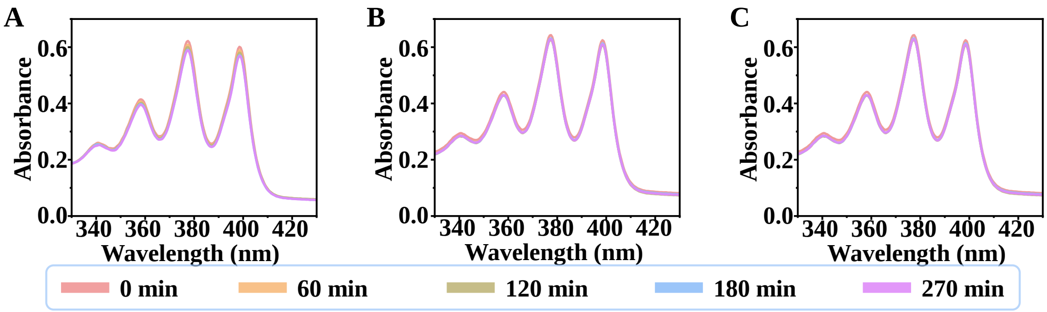

Fig.S14. Absorption spectral changes of ABDA (50 μM in H_2O) in the presence of NP1 (A), NP2 (B) and NP3 (C) without H_2O_2. Concentrations of NP1-NP3: 2 μM based on Ru1-Ru3.

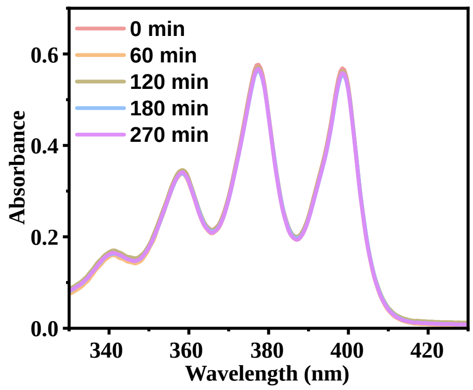

Fig.S15. Absorption spectral changes of ABDA (50 μM in H_2O) in the presence of only H_2O_2 (200 μM).

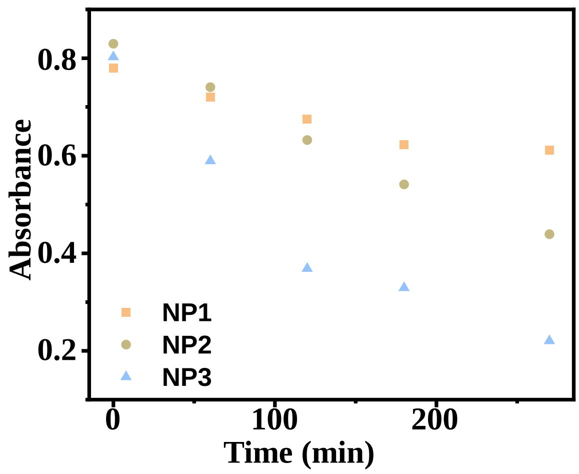

Fig.S16. Absorption spectral changes of ABDA (50 μM) in water at 378 nm in the presence of NP1-NP3 (2 μM based on Ru1-Ru3) and 200 μM H_2O_2.

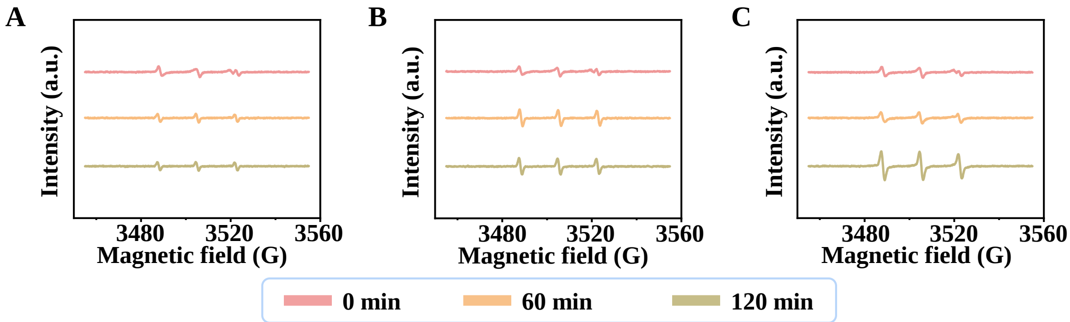

Fig.S17. EPR spectra of NP1 (A), NP2 (B), and NP3 (C) in the presence of H_2O_2 (200 μM) using TEMP (50 mM) as a $^1O_2$ spin trapping agent. Concentrations of NP1-NP3: 4 μM based on Ru1-Ru3.

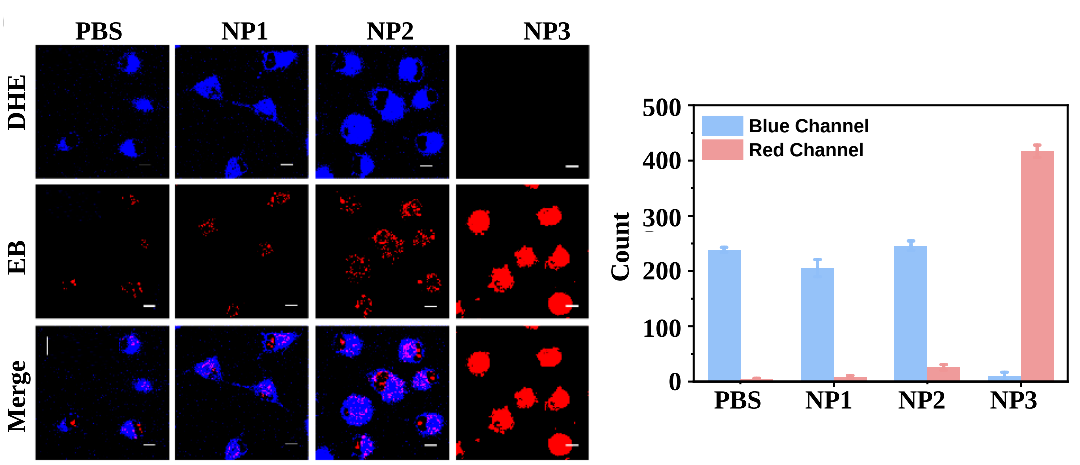

Fig.S18. Confocal laser scanning microscope (CLSM) images of intracellular $O_2^{\cdot-}$ levels of A549 cells treated by PBS or NP1-NP3 (4 μM based on Ru1-Ru3) using DHE as the probe. DHE with blue fluorescence can be oxidized by $O_2^{\cdot-}$ to form ethidium (EB) with bright red fluorescence. Scale bars: 10 μm.

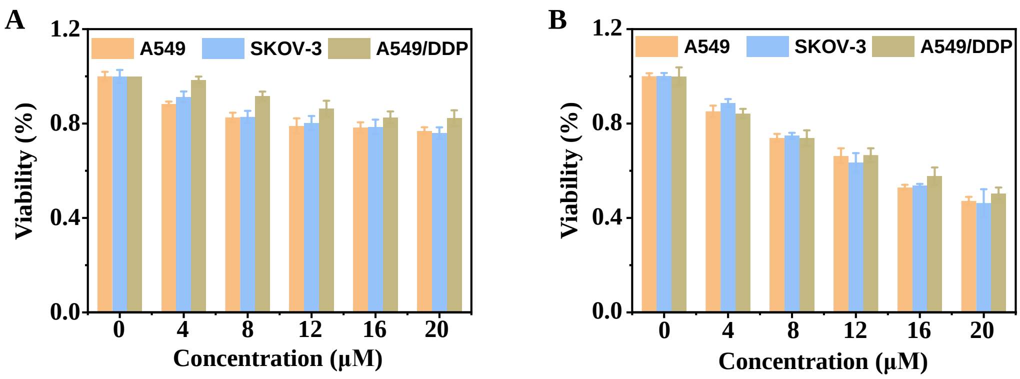

Fig.S19. Cytotoxicity of NP1 (A) and NP2 (B) towards A549, SKOV-3 and A549/DDP cells.

Table S1. IC_{50} values (μM, based on Ru1-Ru3) towards different cells

	A549	SKOV-3	A549/DDP
NP1	>20	>20	>20
NP2	15.8 ± 2.4	18.6 ± 1.1	19.1 ± 0.9
NP3	3.9 ± 1.3	3.6 ± 0.9	4.5 ± 0.7

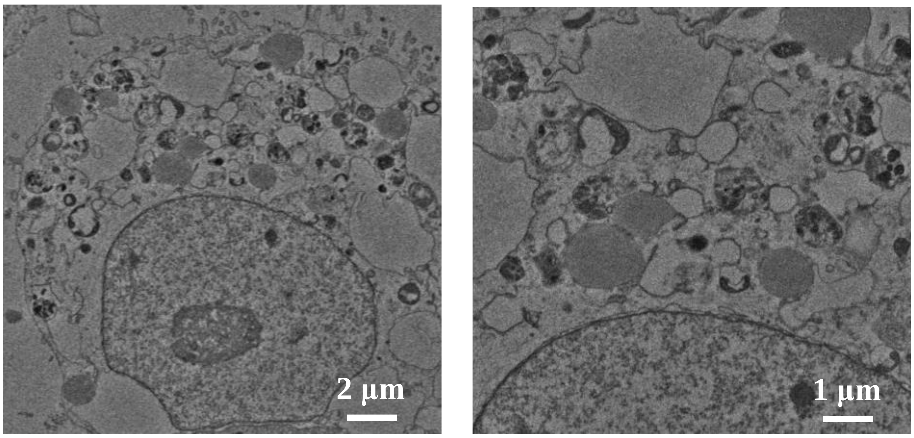

Fig.S20. The biological transmission electron microscopy images of A549 cells after incubation with NP3 (4 μM based on Ru3).

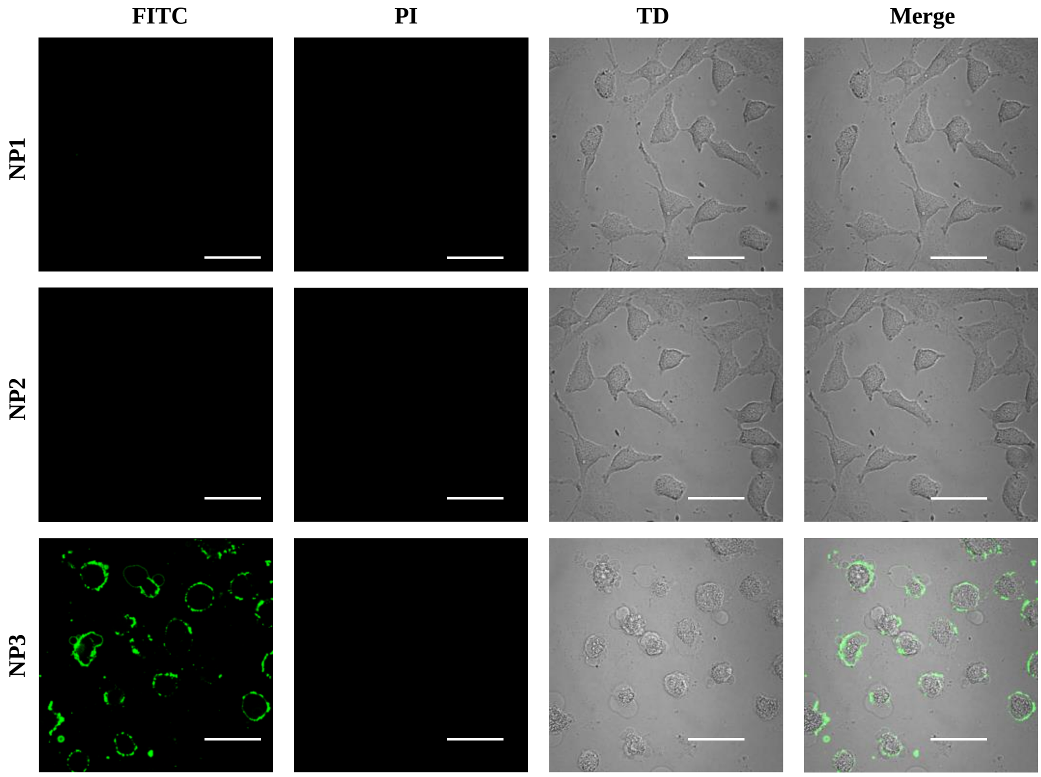

Fig.S21. CLSM images of annexin V-FITC and PI staining results of A549 cells treated with PBS, NP1, NP2 or NP3 (4 μM based on Ru1-Ru3). Scale bars: 50 μm.

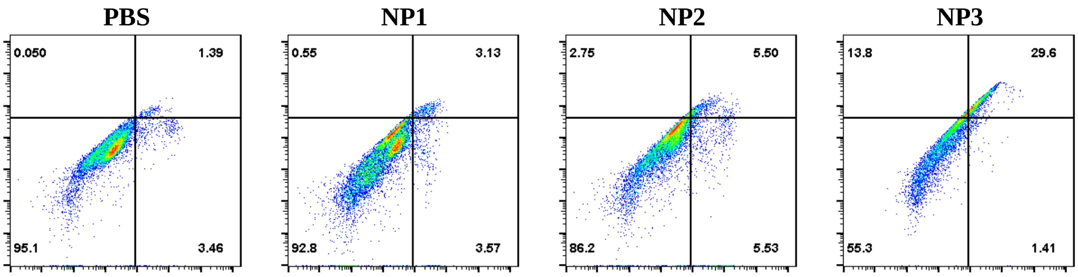

Fig.S22. Flow cytometry results of A549 cells treated with PBS, NP1, NP2 or NP3 (4 μM based on Ru1-Ru3) and stained by annexin V-FITC and PI.

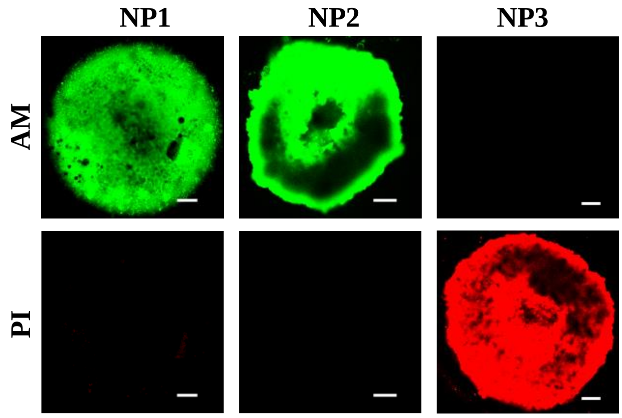

Fig.S23. A549 3D MCSs images treated with NP1-NP3 (10 μM based on Ru1-Ru3), followed by co-staining with calcein-AM and PI. Scale bars: 50 μm.

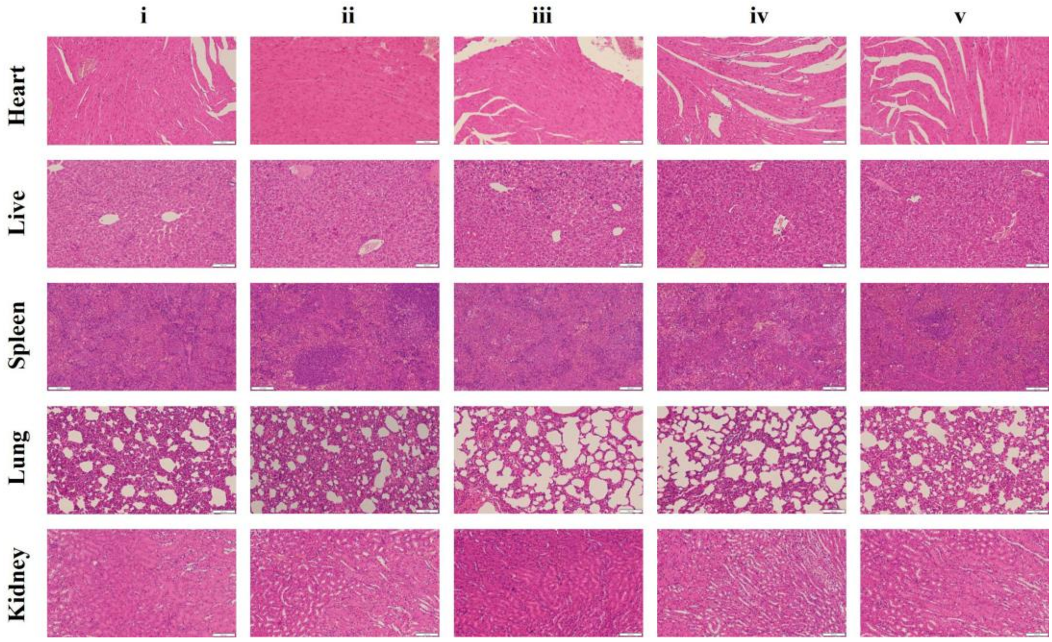

Fig.S24. H&E staining images of heart, liver, spleen, lung, and kidney of mice after different treatments for 16 days. Scale bars: 200 μm.

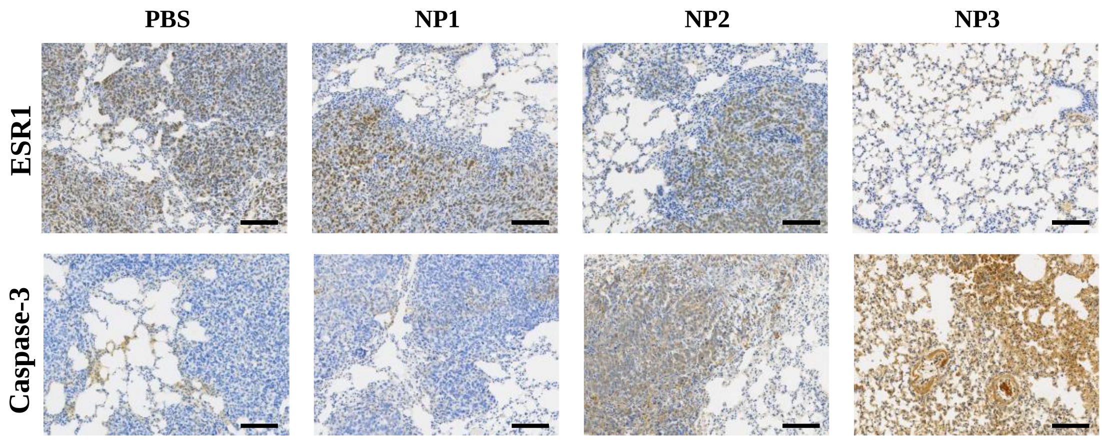

Fig.S25. Immunohistochemical (IHC) stained images of mice lungs after different treatments. Scale bars: 100 μm.

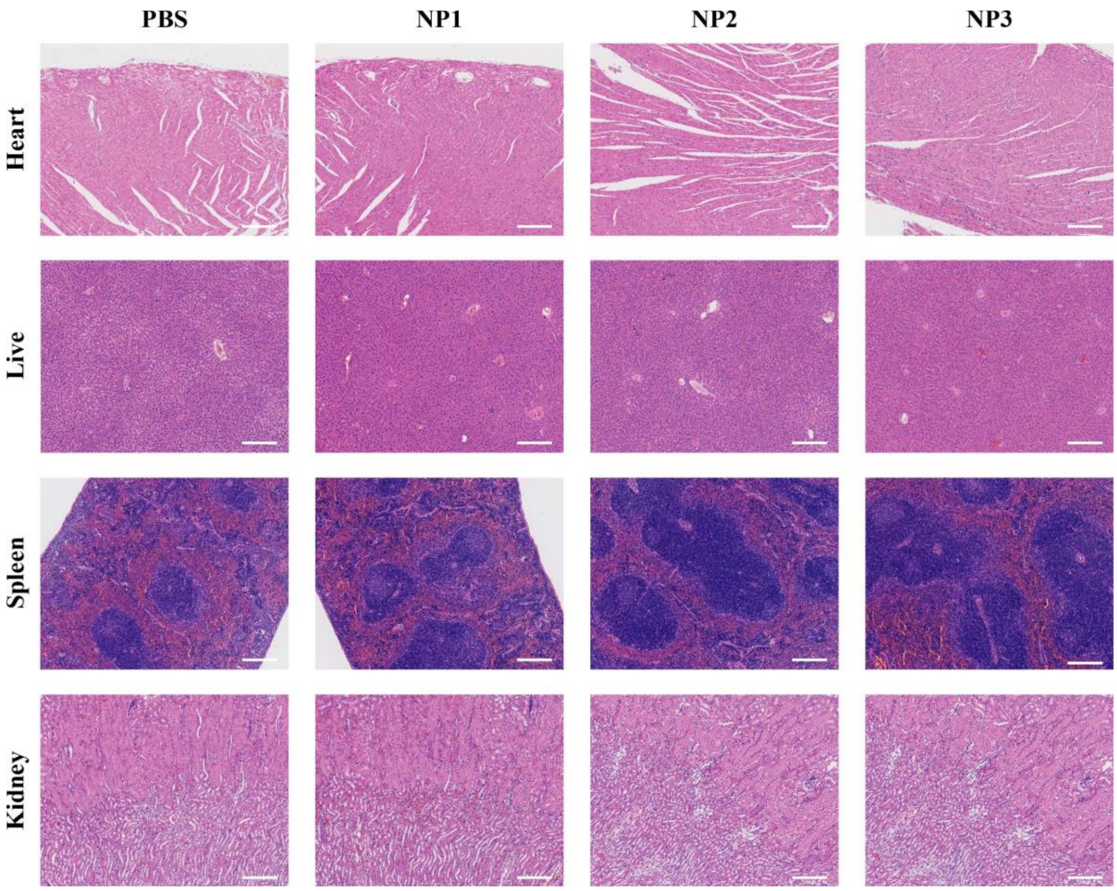

Fig.S26. H&E stained images of major organs (heart, liver, spleen, and kidney) of mice after different treatments for metastatic tumor model. Scale bars: 200 μm.

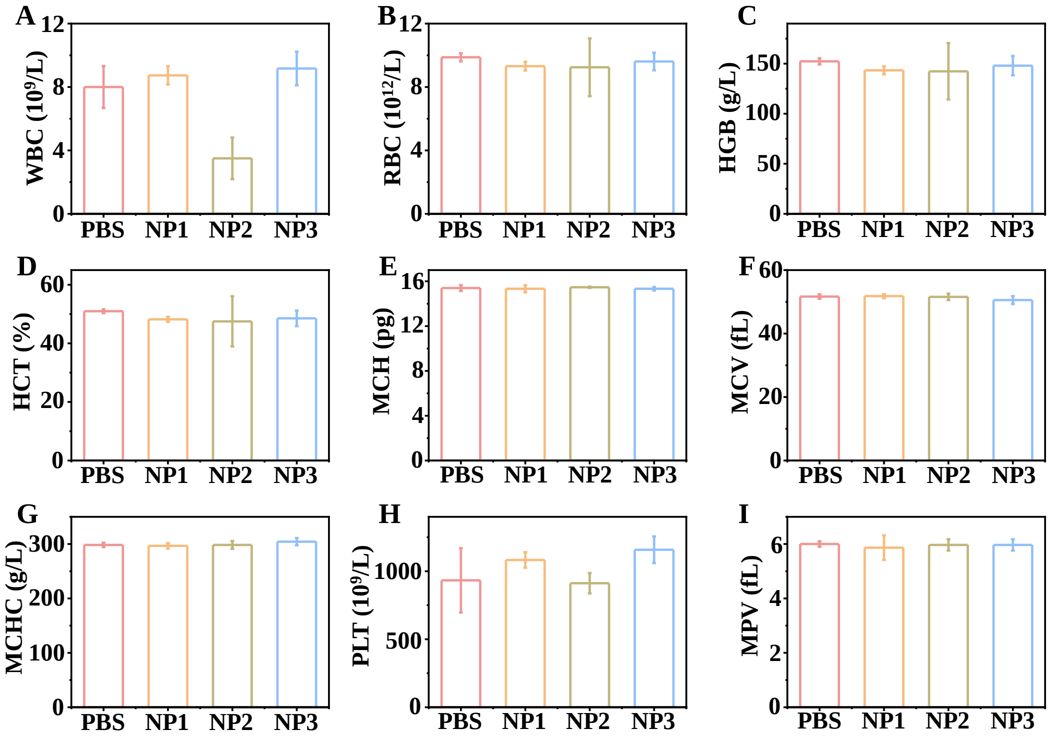

Fig.S27. Blood routine examination of female BALB/c mice after treatment with PBS or NP1-NP3. (A) White blood cells (WBC), (B) Red blood cells (RBC), (C) Hemoglobin (HGB), (D) Hematocrit (HCT), (E) Mean corpuscular hemoglobin (MCH), (F) Mean corpuscular volume (MCV), (G) Mean corpuscular hemoglobin concentration (MCHC), (H) Platelets (PLT) and (I) Mean platelet volume (MPV). The statistic was based on three mice per data point.

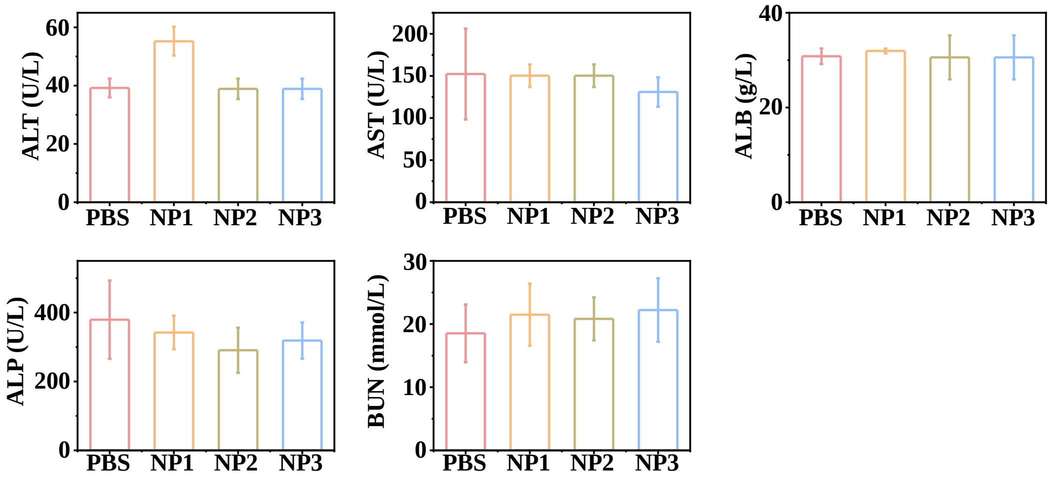

Fig.S28. Blood biochemical examination of female BALB/c mice after treatment with PBS or NP1-NP3 to assess ALT (alanine aminotransferase), AST (aspartate aminotransferase), ALB (albumin), ALP (alkaline phosphatase), and BUN (urea nitrogen). The statistic was based on three mice per data point.